Nano Energy 40 (2017) 34–41

Contents lists available at ScienceDirect

Nano Energy

journal homepage: www.elsevier.com/locate/nanoen

Full paper

The interplay between solid electrolyte interface (SEI) and dendritic lithium growth

Bingbin Wu[a], Joshua Lochala[a], Tyler Taverne[b], Jie Xiao[a,*]

[a] Department of Chemistry and Biochemistry, University of Arkansas, Fayetteville, AR 72701, United States
[b] Department of Mechanical Engineering, State University of New York (SUNY) Polytechnic Institute, 100 Seymour Rd, Utica, NY 13502, United States

ARTICLE INFO

Keywords:
SEI
Dendritic Li
Cell short
Li metal batteries
Energy storage

ABSTRACT

Li dendrite formed in Li metal batteries can be categorized into two different types. One is the detrimental Li dendrite that heads towards the separator with a potential to short cell. The other is the ill-defined fibrous Li formed within bulk Li metal. The detrimental Li dendrite may cause cell short, while the other dendrites, covered by SEI, mainly increase cell impedance and terminate the cell operation, most often, before any "short" really happens. Without decoupling these two different Li dendrites, it is hard to develop any effective approach to realize both stable and safe Li metal batteries. Herein, a straightforward approach is proposed to induce the growth of detrimental dendritic Li so the cells are "shorted" frequently and consistently. Based on this new protocol, various electrolytes are revisited and the SEI derived are compared and quantified, providing new insights for addressing the challenges in rechargeable Li metal battery technologies.

1. Introduction

The energy of next-generation batteries employing Li metal anode is projected to be about twice that of the conventional Li-ion batteries [1–4]. The energy gain mainly comes from Li metal anode which has the lowest negative electrochemical potential, high theoretical specific capacity and light weight [5]. However, Li metal is thermodynamically instable in the electrolyte and a passivation film or so called SEI layer forms unavoidably on Li surfaces which prevent the further reaction between Li and electrolyte [6]. Although Li metal is temporarily protected by nanoscale SEI layers, during repeated cycling, Li anode experiences large volume change [7], which means its surface area increases drastically. The newly exposed Li surfaces quickly react with the electrolyte, form new SEI layers and gradually increase the whole cell impedance [8]. The insulating SEI layers disrupt the uniform distribution of the electrical field on the metal anode thus the growth rate of micro/nano Li crystals become uneven, forming porous or fibrous Li. The surface areas of Li continue to increase and produce more SEI layers [9]. The original dense Li metal are gradually "corroded" to porous structures with SEI layers accumulated on all the exposed Li surfaces [10]. Continuous SEI formation irreversibly consumes electrolyte in the cell. Once the electrolyte is depleted, the cells also malfunction. In liquid cells, Li protection means the prevention of both potential dendrite penetration [11] through the separator and Li "corrosion" [7,12] towards the bulk Li metal. The former causes safety concern, while the latter accumulates cell impedance and drains the electrolyte that accelerate the capacity degradation.

While not all of the Li dendrites will short the cell, Li corrosion always happen and substantially increases cell impedance [13], which terminates the cell operation much earlier than cell short happens, if any. Improved Columbic efficiency and cycling stability mainly reflect the slowdown of SEI accumulation/impedance buildup during cycling [14]. It does not necessarily mean that those methods will also prevent the dendrite-caused short at extreme conditions e.g., high rate, low temperature or in the presence of impurities [15]. Most often, the cells already malfunction before any detrimental Li dendrite forms and eventually short the cell [7,16]. The majority of the published methods effectively mitigate the continuous SEI/impedance accumulation issue [17,18]. However, the effectiveness of the approaches to prevent cell short caused by dendrite penetration is uncertain since none of the reported control cells fails because of shorting. An effective testing approach is urgently needed to decouple the dangerous Li dendrite growth and Li corrosion.

Herein, a convenient method is proposed to induce Li dendrite to "short" the cell consistently. Different electrolytes are revisited by using the proposed method and the resistance of SEI films derived from various electrolytes are quantified and compared to understand the fundamental mechanisms that control the Li growth.

* Corresponding author.
E-mail address: jiexiao@uark.edu (J. Xiao).

http://dx.doi.org/10.1016/j.nanoen.2017.08.005
Received 5 July 2017; Received in revised form 1 August 2017; Accepted 2 August 2017
Available online 04 August 2017

2. Experimental

2.1. Electrolytes preparation

Dissolving certain amount of lithium salt ($LiPF_6$, LiTFSI) into required solvents or their combinations (carbonate based solvents: EC, DMC; ether based solvents: DME, DOL) in an argon filled glove box ($O_2 < 0.5$ ppm, $H_2O < 0.5$ ppm, MBRAUN). The prepared eleven electrolytes include 1 M $LiPF_6$-EC/DMC (1/1, by volume), 4 M $LiPF_6$-EC/DMC (1/1, by volume), 1 M LiTFSI-DME, 4 M LiTFSI-DME, 1 M LiTFSI-DOL, 4 M LiTFSI-DOL, 1 M LiTFSI-DME/DOL (1/1, by volume), 2 M LiTFSI-DME/DOL (1/1, by volume), 3 M LiTFSI-DME/DOL (1/1, by volume), 4 M LiTFSI-DME/DOL (1/1, by volume) and 5 M LiTFSI-DME/DOL (1/1, by volume).

2.2. Cell assemble and tests

2032 type Li/Li symmetric cells were assembled in the argon filled glove box using either Celgard2500 (thickness: 25 μm) or glass microfiber filter 691 (thickness: 250 μm) as the separator. In Li/Li symmetric cells, one Li disk (250 μm thick from MTI) has a diameter of 14 mm while the other is 15.5 mm in order to easily align two Li metal pieces. 60 μL of electrolyte is used when Celagrd2500 is used, while 100 μL electrolyte for glass fiber separator. The Li/Li cells were constant-current charged/discharged to 0.5 mA h cm^{-2} with 0.25 mA cm^{-2} (0.5 C) of current density at 25 °C using LANHE battery tester (CT2001A).

2.3. Characterizations

The morphology of glass fiber separator is observed by scanning electron microscope (VEGA-II, Tescan). Optical microscope (ME-520T, Amscope) is used in glove box to characterize the separators after cycling. EIS tests of Li/Li symmetric cells are performed with CHI660E (CH Instruments Ins.) at frequency ranging from 1 MHz to 0.5 Hz at 25 °C. The Li/Li cells for EIS tests are assembled using eleven different electrolytes and charged to 0.5 mA h cm^{-2} with a current density of 0.25 mA cm^{-2} (0.5 C) at 25 °C. The EIS impedances of the cells before and after deposition and after being stored for 1 week are recorded. Each EIS measurement has been repeated with highly reproducible results.

3. Results and discussion

3.1. Decoupling SEI buildup-caused cell failure and dendritic Li-induced cell short

3.1.1. Cell short scenarios

There are a few different scenarios that may cause cell shorts. Li dendrite penetration through Celgard is only one of the possible reasons which is also the focus of this work. In addition to Li dendrite-caused short, aggregated Li metal branches continuously press the Celgrad film which may also lead to soft short. For Celgard 2500, the tensile strength of transverse direction is only 135 kg cm^{-2}, while it is 1055 kg cm^{-2} at the machine direction [19]. If the Li agglomerate accidently forms at the weak tensile strength direction of Celgard and the cell undergoes volume expansion during cycling, the large Li aggregates may be "pushed" through the separator membrane causing short as well. Overcharge will induce the growth of Li agglomerates [20]. Over discharge may dissolve Cu from the anode current collector and generate Cu^{2+} ions that deposit on the cathode as an "impurity" particle [21]. Similarly, if there is any impurity such as a dust particle pre-existing in the vicinity of separator, during cycling, this impurity particle may also get the cell short [15]. All these possible causes need to be considered for the safety operation of Li-ion and Li metal batteries. This work focuses on the discussion of cell shorting caused by dendritic Li since the targeted system is Li metal batteries. However, all the aforementioned issues may still play roles in affecting the cell safety and should be considered in reality.

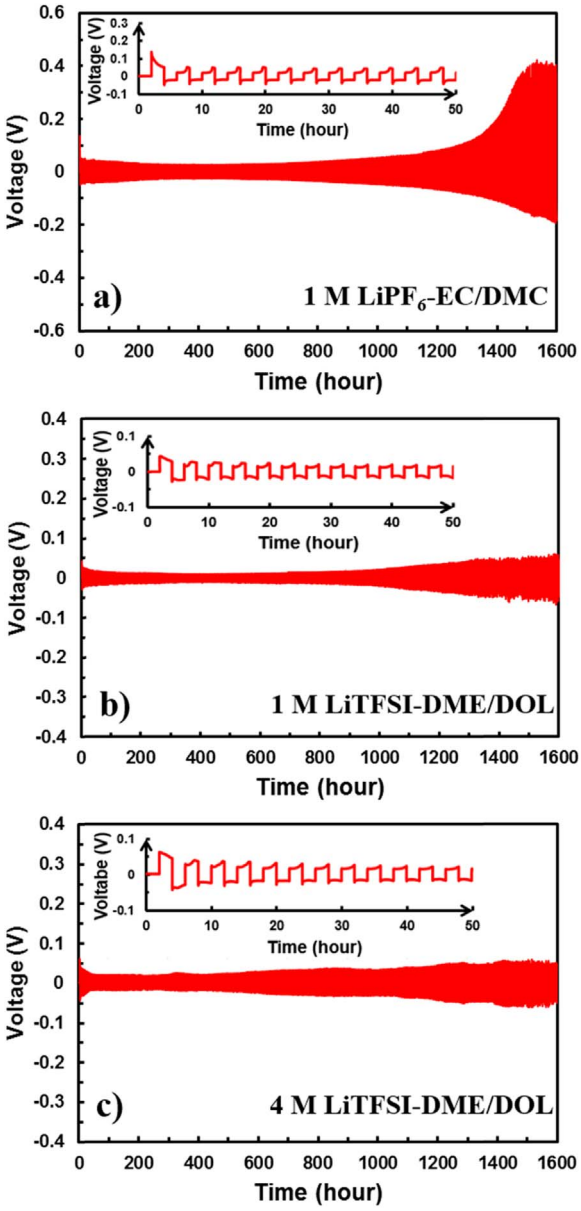

Fig. 1. Cycling behaviors of Li/Li symmetric cells using Celgard 2500 as the separator in (a) 1 M $LiPF_6$-EC/DMC (1/1), (b) 1 M LiTFSI-DME/DOL (1/1) and (c) 4 M LiTFSI-DME/DOL (1/1) relatively. The cells are charged/discharged at 0.25 mA cm^{-2} to 0.5 mA h cm^{-2} at 25 °C.

3.1.2. Why it is difficult to capture dendrite-caused short in coin cell testings

Most lab R & D tests are using Celgard membrane as the separator. For example, in Fig. 1, Li/Li symmetric cells are tested in three different electrolytes: 1 M $LiPF_6$-EC/DMC, 1 M and 4 M LiTFSI-DME/DOL. The former is the conventional carbonate-based electrolyte for Li-ion batteries, while the latter is the standard recipe for Li-S batteries [22,23]. 4 M LiTFSI-DME/DOL is also tested because of the recent interests on the unique SEI properties derived from concentrated electrolytes [14,24,25]. Symmetric cells tested in either carbonate or ether-based electrolytes show very stable cycling for at least 1000 h (Fig. 1). The voltage polarization of Li/Li cells cycled in carbonate solvents is 25 mV (after 50 h) in Fig. 1(a), higher than that those in ether-based solvent (ca. 13 mV in Fig. 1(b)) indicating a higher resistance of SEI derived from EC/DMC [26]. After about 1000 h cycling, the polarization of the

cell in 1 M $LiPF_6$-EC/DMC shows a steady increase and reached 149 mV at 1500 h (Fig. 1(a)). Cells cycled in 1 M LiTFSI-DME/DOL (Fig. 1(b)) show a very small over potential at 13 mV in the beginning which increases slightly to 46 mV even after 1500 h. Concentrated electrolyte, 4 M LiTFSI-DME/DOL, also displays a stable cycling for a long while, followed by polarization increase, reflecting to the accumulation of cell impedances (Fig. 1(c)). The increase of polarization in all the tested cells are in accordance with the Li corrosion process in which insulating SEI layers are continuously generated and accumulated due to the formation of new Li surfaces during each cycling. In other words, none of the failed cells in Fig. 1 are caused by short. Otherwise, the voltage of the cells should drop to close to 0 V simply according to the Ohm's law. The experiments in Fig. 1 have been repeated for quite a few times and none of the cells show "short" phenomenon.

At standard testing condition (0.25 mA cm^{-2} current density and 0.5 mA h cm^{-2} capacity in this case), it is hard to capture any dendrite-caused cell short. The main reason is because of the use of Celgard as the separator. For Celgard2400 or 2500, the pores on the membranes are in the nano-range of only 100–200 nm [27]. For a dendrite to short the cell, it has to continuously grow towards the separator without any interruption and target for the nanopores and eventually penetrate through the membrane. This is a very low-chance phenomenon at regular testing conditions. For Celgard2325, the triple layer configuration makes this kind of cell short even more difficult, not mentioning that ceramics are further coated to the polypropylene outer layers in the recent versions [28]. At extreme testing conditions such as deep deposition of Li (Supplementary information Fig. S1) or high current density (Fig. S2), cell short sometimes can be seen without consistence. The occurrence of the dendrite-caused short is a randomly happening phenomenon even at those extreme testing conditions. Therefore, although the use of Celgard helps to protect Li metal cells from short, it also complicates the effective evaluation of new approaches targeted to eliminate the dangerous Li dendrite.

3.1.3. Inducing the growth of the detrimental Li dendrite

In order to induce the growth of Li protrusion, glass fiber membrane (filter paper) has been employed to replace Celgard as the separator. Glass fiber (Fig. 2(a)) consists of quartz and the fibers are randomly tangled together forming a wide range of pore sizes, some of which reach hundreds of microns (Fig. 2(b)). These large pores across glass fibers provide sufficient space for dendritic Li to pass through.

Fig. 2(c) shows the cycling result of Li/Li symmetric cell tested at exactly the same conditions in Fig. 1(c) except that glass fiber membrane is used as the separator. In the same 4 M LiTFSI-DOL/DME, the cell with glass fiber separator undergoes a sudden voltage drop and reaches 5 mV (close to 0 V) after only 130 h. In Fig. 1(c) where Celgard is used as the separator, the stable cycling lasts for 1600 h without any voltage drop. To confirm that the cell after the sharp voltage drop is caused by the "short", two filter papers are stacked together as an entire separator (illustrated in Fig. 2(d)). The same sudden voltage drop (Fig. 2(e)) is still observed after cycling for about 750 h in the cell with double-layer separator. From the disassembled cell, black mossy Li (Fig. 3(a)) is found on the surface of cycled Li disk and outer side of glass fiber (Fig. 3(b)), consistent with the Li pulverization during cycling [29]. The inner side of the two glass fibers contains many black spots (Fig. 3(c)), which are in fact dendritic Li growing through the two stacked glass fibers (Fig. 3(d)). The black aggregates (Fig. 3(g)) consist of numerous entangled Li dendrites, some of which grow along the fibers (Fig. 3(g)). In certain areas, black Li agglomerates are found to form and push against glass fiber separator (Fig. 3(e)) and some of them already "break out" from the thick glass fiber layer (Fig. 3(f)), indicating that the stress localized on the Li particles is very strong. These observations in Fig. 3 confirm that the sudden voltage drop in Fig. 2 is the signal of cell short caused by the Li dendrite. The cell voltage is not exactly 0 V because the short is "soft", where current flows only through a resistance showing a constant cell voltage [30].

3.2. The Interplay between SEI and Li metal growth

3.2.1. Revisit different electrolytes using glass fiber separator

Using glass fiber separator, various electrolytes with different concentrations are re-evaluated in terms of their abilities to "stop" the growth of Li dendrites towards the separators. Fig. 4 compares three representative concentrated electrolytes with more examples to be discussed in the following section. For carbonate electrolytes, the cell tested in 4 M $LiPF_6$-EC/DMC (Fig. 4(a)) is short after only 280 h cycling. When ether-based electrolytes are compared, the one cycled in 4 M LiTFSI-DOL has very low over potential at ca. 10 mV but gets short

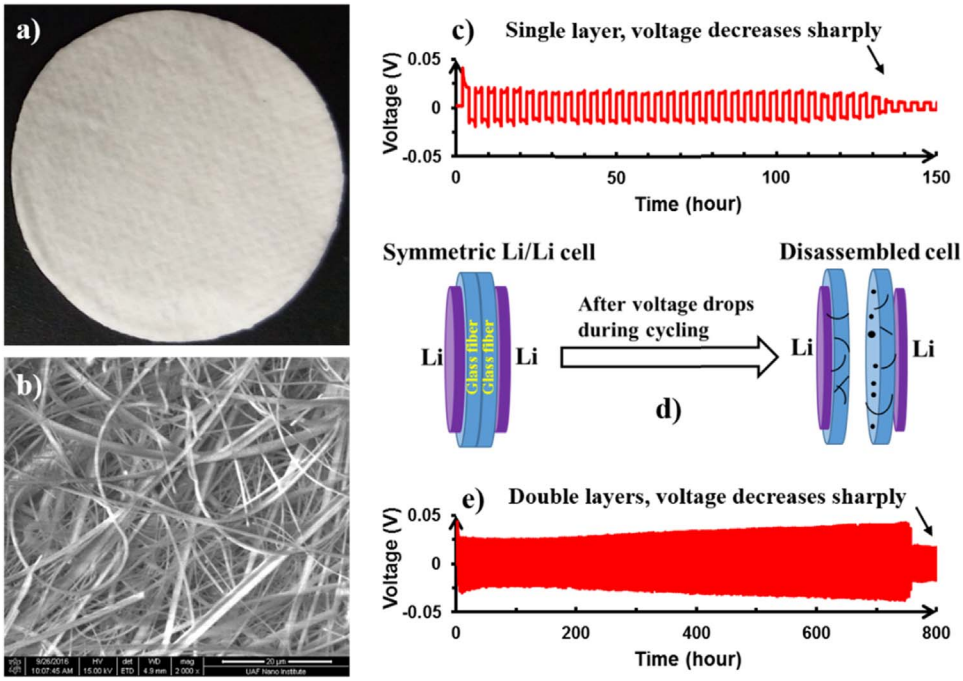

Fig. 2. (a) Digital photograph, (b) SEM image of glass fiber, (c) cycle behavior of Li/Li symmetric cells using single layer glass fiber separator, (d) Illustration of a Li/Li cell using two stacked glass fiber separators to evaluate cell short behavior and (e) the corresponding cycling behavior of (d) in 4 M LiTFSI-DME/DOL (1/1). The cells are charged/discharged at 0.25 mA cm^{-2} to 0.5 mA h cm^{-2} at 25 °C.

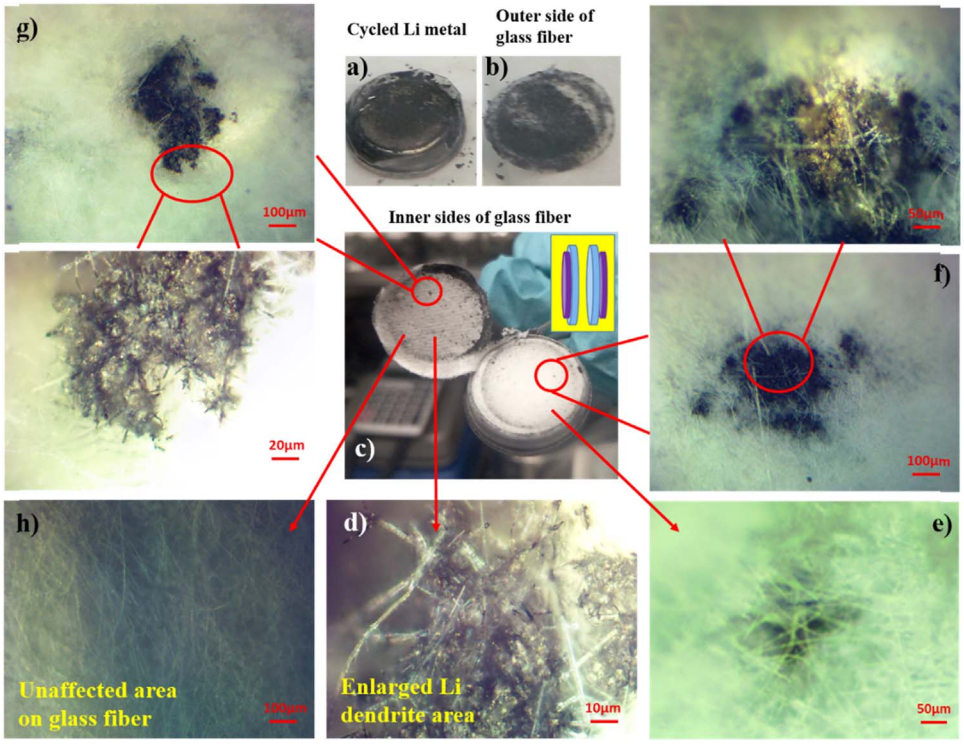

Fig. 3. Optical microscopy images of the shorted Li/Li symmetric cell in Fig. 2(e). (a) Cycled Li metal, (b) one side of the glass fiber separator attached to Li metal side, (c) inner sides of two glass fiber separators disassembled (inset: Li/Li cells with two stacked glass fiber separators). (d) Enlarged black spot area in (c) indicates some of Li dendrite grows along the fibers of the separator, (e) Li agglomerate formed underneath glass fiber. (f) Li aggregate breaks out from separator and its enlarged image; (g) another Li aggregate on the glass fiber separator and its enlarged image showing obvious dendritic structures; (h) unaffected area of the glass fiber separator.

quickly after 200 h (Fig. 4(b)). If switching to the pure DME solvent (Fig. 4(c)), the cell demonstrates a higher polarization (33 mV) than in DOL but no short is seen, indicating that the SEI resistance derived from DME is higher than from DOL.

Table 1 compares eleven different types of electrolytes tested at the same conditions as those discussed in Fig. 4. A general rule is found that 1) cells cycled in the concentrated electrolytes usually get short earlier than in their regular 1 M version except for pure DME-based electrolytes and 2) most of the shorted cells have already displayed low over potentials during early cycling.

SEI layers are mainly derived from the decomposition of the solvents [31]. In concentrated electrolytes, due to the reduced amount of solvent molecules, SEI layers formed during each cycle are thinner and have lower resistances [14,24]. Accordingly, the ability of these "weak" SEI layers in concentrated electrolytes to terminate the Li dendrite propagation is poor. Fig. 5 further compares LiTFSI-DME/DOL with concentrations ranging from 1 M to 5 M. In general, cells tested in 4 or 5 M LiTFSI-DME/DOL get short earlier than in 2 or 3 M concentrations, while the one tested in 1 M LiTFSI-DME/DOL does not short at all. While not all the cells in parallel testing get short at exactly the same time, highly concentrated electrolytes probably forming thinner SEI layers [32,33], are more difficult to "stop" the continuous dendrite growth. For the SEI formed between concentrated electrolytes and electrodes (not limited to Li anode), in addition to the significantly reduced decomposition of free solvent molecules, the affinity of anions [34] and the precipitation constant of the salts [25] under the electrical field all need to be considered. On the other hand, the low resistant SEI layers derived from concentrated electrolytes, although cannot "stop" dendrite formation, will largely slow down the impedance buildup process in the cells. This explains why in literature, the cycling stability of Li metal (Celgard used as the separator) is always significantly improved in concentrated ones compared with their regular 1 M counterpart [14,35]. It is noticed that cells tested in LiTFSI-DME never gets short regardless of the electrolyte concentrations (Fig. S3), suggesting that SEI resistance derived from LiTFSI-DME is very high.

From the above discussion, it is clear that conflicting requirements exist for the resistances of SEI layers formed at different parts of the dendritic Li. For the SEI covering the top of Li sprouts, a highly resistant SEI is desired in order to slow down and eventually stop this continuous dendrite propagation towards the separator. For the SEI formed on the surface of "non-detrimental" Li dendrites i.e., those that do not threaten to penetrate the separator, a low resistant SEI is preferred to alleviate the increase of cell impedance caused by SEI accumulation. A single additive or approach, obviously, cannot meet both conflicting requirements.

3.2.2. *Quantification of SEI resistances in different electrolytes*

The over potential usually reflects the total impedance of the whole cell including the contributions from the electrolyte, SEI film, charge transfer reaction and diffusion step. In order to extract the information directly related with SEI layers, Electrochemical Impedance Spectroscopy (EIS) has been applied to analyze eleven different electrolytes discussed in Table 1. The Li/Li cells are charged to 0.5 mA h cm^{-2} to form fresh SEI. The cell impedance before and after Li deposition are both collected. After that, the cell is stored at room temperature for one week, followed by recording the cell impedance again (see details in Fig. 6(a)). Every EIS experiment has been repeated twice and the results are reproducible (Fig. S4). Fig. 6(b) only shows the representative EIS results obtained from two parallel tests in 4 M LiTFSI-DME/DOL (cell 1 and cell 2 in Fig. 6(b)), which are almost duplicating each other. These plots are well fitted by an equivalent circuit (Fig. 6(c)), consisting of impedance from electrolyte (R_s), SEI film at Li metal interface (R_{sei}) and charge transfer reaction (R_{ct}) and their corresponding constant phase elements (CPE): CPE_{sei} and CPE_{ct}. All the electrolytes are tested in the cells using the same protocol. The parallel EIS measurements and their fitted results can be found in Fig. S4 and Table S1.

To simplify the discussion, R_{sei} before and after Li deposition are referred as R_0 and R_1, respectively. R_{sei} of the cell after being stored for 1 week is referred as R_2. After Li deposition, SEI resistance, R_1, always becomes less than the original R_0 in most of the tests because of the increase of Li surface areas during deposition. After storage, SEI resistance, R_2, is increased compared to R_1 in most cases due to the SEI thickening (Fig. 6(b) and Fig. S4). The difference between R_2 and R_1 is

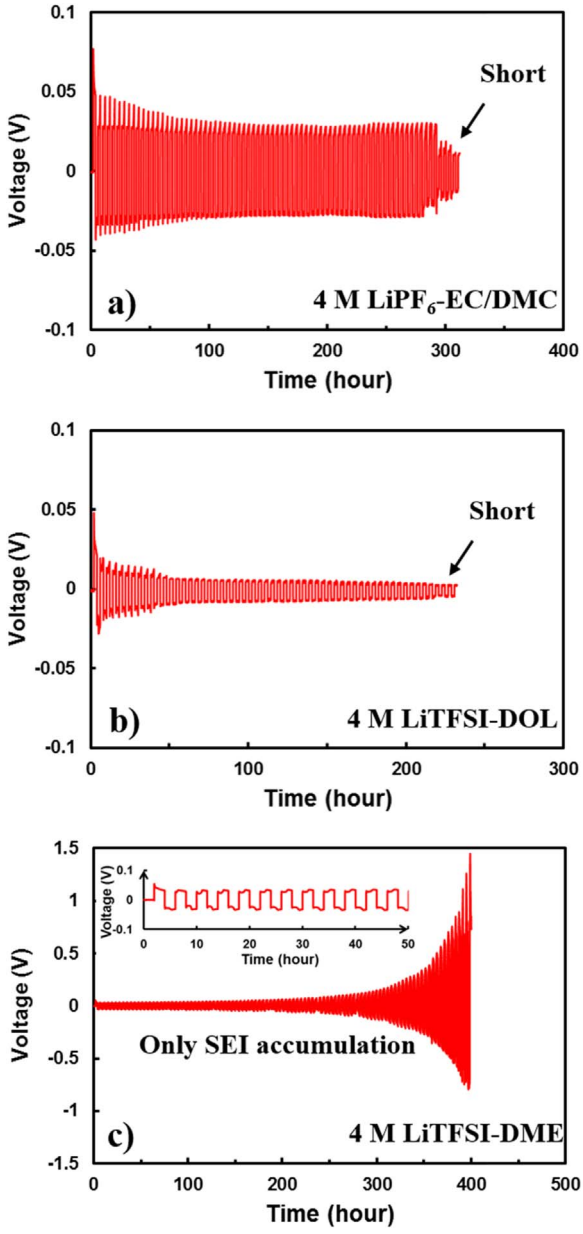

Fig. 4. Cycling behaviors of Li/Li symmetric cells using glass fiber separator in concentrated electrolytes. (a) 4 M $LiPF_6$-EC/DMC (1/1); (b) 4 M LiTFSI-DOL and (c) 4 M LiTFSI-DME. The cells were constant charged/discharged at 0.25 mA cm^{-2} to 0.5 mA h cm^{-2} at 25 °C.

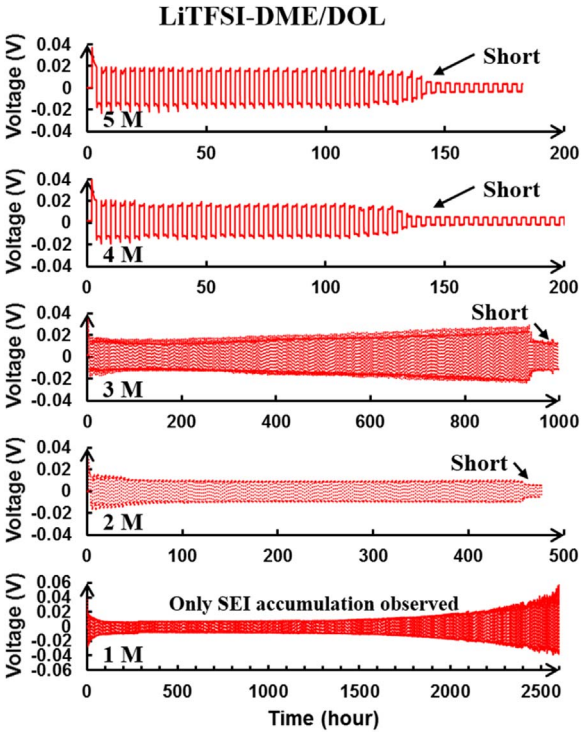

Fig. 5. Cycling behaviors of Li/Li symmetric cells using glass fiber separators tested in different concentrations of LiTFSI-DME/DOL electrolytes. The cells are all charged/discharged at 0.25 mA cm^{-2} to 0.5 mA h cm^{-2} at 25 °C.

normalized by the geometric area S_0 of the electrode i.e., $(R_2\text{-}R_1)/S_0$, which can be used solely to indicate the SEI film resistances derived from the electrolytes without the interruption of surface area variations of Li in different cells. Fig. 6(d) compares eleven different electrolytes (the same as in Table 1) in terms of their $(R_2\text{-}R_1)/S_0$ and R_2/S_0. Combined with the results from Table 1, an interesting finding is that the cells tested in the electrolytes (highlighted by yellow) with $(R_2\text{-}R_1)/S_0 < 10\ \Omega\ cm^{-2}$ and $R_2/S_0 < 50\ \Omega\ cm^{-2}$ are the ones that always short after cycling. This means that the highlighted electrolytes produce low resistance SEI which helps to extend the reversible cycling of Li metal. If $(R_2\text{-}R_1)/S_0 > 10\ \Omega\ cm^{-2}$ and $R_2/S_0 > 50\ \Omega\ cm^{-2}$, the cells fail mainly due to impedance increase instead of short after cycling, indicating that the electrolytes used derive high-resistance SEI layers. This quantification method can be conveniently used to quickly evaluate various electrolytes for different applications. Especially for the electrolytes to be used in rechargeable Li metal batteries, in addition to the stability, viscosity and ionic conductivity etc, the balances of SEI properties derived from different solvents may also need to be considered.

Table 1
Comparison of over potentials and failure modes of Li/Li cells tested in various electrolytes with glass fiber used as the separator.

Electrolytes	Over potential in the early stage (mV) (after 50 h stable cycling)	Over potential when cell fails (mV)	Failure mode
1 M $LiPF_6$-EC/DMC	33	737	Impedance buildup
4 M $LiPF_6$-EC/DMC	29	10	Short
1 M LiTFSI-DME	58	3128	Impedance buildup
4 M LiTFSI-DME	33	4016	Impedance buildup
1 M LiTFSI-DOL	11	4	Short
4 M LiTFSI-DOL	10	4	Short
1 M LiTFSI-DME/DOL	10	53	Impedance buildup
2 M LiTFSI-DME/DOL	10	5	Short
3 M LiTFSI-DME/DOL	14	11	Short
4 M LiTFSI-DME/DOL	16	5	Short
5 M LiTFSI-DME/DOL	16	4	Short

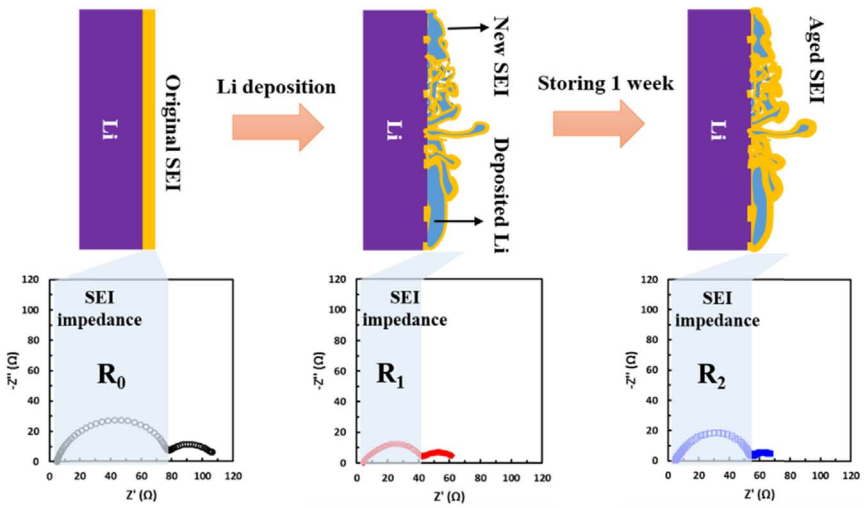

Fig. 6. (a) The proposed EIS measurement protocol to quantify SEI impedances derived from different electrolytes. EIS measurements are conducted before and after deposition and after being stored for 1 week at 25 °C in Li/Li symmetric cells. (b) Complex plane plots of two Li/Li cells in 4 M LiTFSI-DME/DOL with glass fiber as the separator and (c) their equivalent circuits used for fitting. Li/Li cells are charged to 0.5 mA h cm^{-2} at 0.25 mA cm^{-2} to deposit fresh Li. EIS measurements of the cells are conducted at 25 °C with an amplitude of 10 mV and frequencies ranging from 1 MHz to 0.5 Hz. The frequency of the first semi circle ranges from 121 kHz to 46 Hz. (d) Normalized resistance (R_0 is the SEI film resistance spontaneously formed on Li metal before applying the electrical field. R_1 is SEI film resistance of cell after depositing. R_2 is the SEI film impedance after being stored for 1 week after Li deposition. S_0 is the electrode area of Li metal anode i.e., 1.54 cm^2). Two parallel tests are conducted for each electrolyte (cell 1: circle marker with dash line; cell 2: square marker with solid line). Highlighted electrolytes on the X-axis are those producing low-resistance SEI layers.

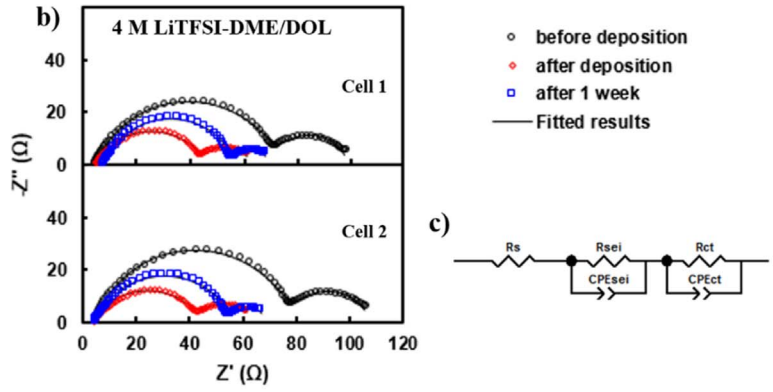

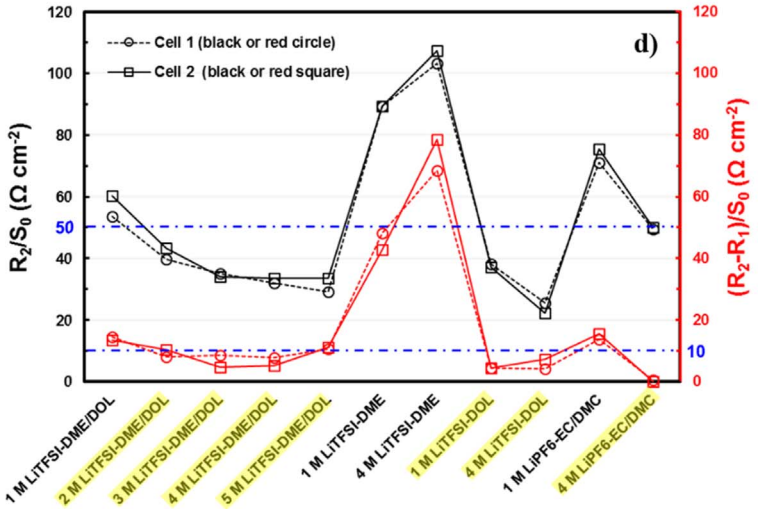

3.2.3. Proposed mechanisms for Li morphology evolution in different electrolytes

The mechanism of Li morphology evolution [36,37] in different electrolytes is proposed in Fig. 7. Regardless of the electrolyte types, the SEI layer formed on the nano-sized tip of any Li dendrite is always "thicker" or more resistant than those on the rest parts of Li. This is because the localized region of increased current densities on the Li tips exacerbates the electrolyte decomposition. Accordingly, the Li growth rate is slower at the forefront of Li dendrite due to the higher SEI impedance.

If the electrolyte used in the cell also happens to produces high resistance SEI (Fig. 7(a)), the SEI impedance on the Li tip easily becomes sufficiently high to discontinue the further growth of Li protrusion (Fig. 7(b)). To balance the charge flow, Li has to sprout from other lower parts of the dendritic Li (Fig. 7(c)) that are covered by relatively lower resistance SEI. The newly formed Li tip at other locations, however, experiences the same "slow down-to-stop" growth due to the formation of high impedance SEI layers on the Li spike. This process repeats and Li curvatures or branches form very quickly (Fig. 7(d)). The Li branches wrapped by the highly resistant SEI layers easily become

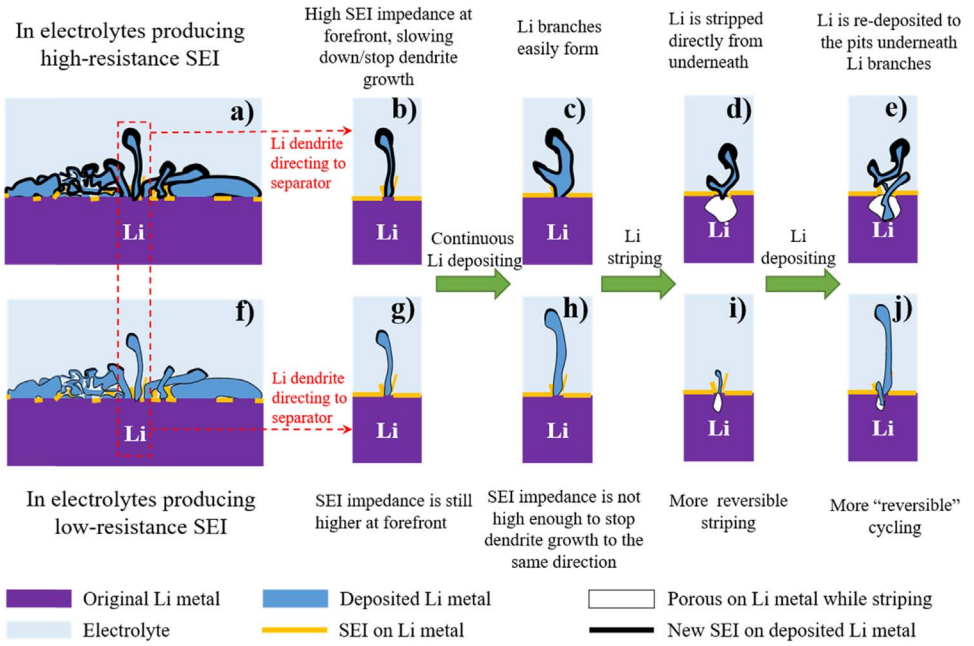

Fig. 7. Schematic illustration of the propose mechanisms of Li dendrite growth. (a–e) In electrolytes generating high-resistance SEI layers and (f–j) in electrolytes generating low-resistance SEI layers.

"dead" by losing the electronic contact with other Li. "Dead" Li branches will not participate in the electrochemical reactions but simply increases the cell impedance. During the subsequent cycling, intact bulk Li underneath the "dead" Li branches will be directly stripped, leaving pits behind (Fig. 7(d)). These pits will also be preferentially "refilled" during deposition through the relatively "weak" SEI (Fig. 7(e)). This process repeats until the whole Li metal lose "activity" or the electrolyte is drained up, whichever comes first. A recent published work on in situ characterization of Li metal morphology change during cycling exactly reflects the pits formation phenomenon directly underneath the Li branches [10]. The electrolytes used in that work belong to the category of producing high impedance SEI as discussed in this work.

In contrast, if the electrolytes generate low resistance SEI (Fig. 7(f)), dead Li branches will not form that quickly. The whole dendritic Li reversibly participates in the electrochemical reaction for an extended time period when Celgard is used as the membrane to prevent the propagation of Li dendrite through the separator (Fig. 7(g) and (h)). Note that SEI layer formed on Li tip is still more resistant than on the rest parts of Li but it is not sufficiently "strong" to terminate the Li growth towards this direction. Therefore, the opportunity of this dendritic Li (heading towards separator) to short the cell is largely increased. Because of the low resistance SEI, reversible electrochemical reaction of each Li dendrite lasts for a longer time, delaying the formation of "dead" Li and pits (Fig. 7(i)). Accordingly, more stable cycling (Fig. 7(j)) will be observed in the cells containing the electrolytes producing low resistance SEI layers, provided that Celgard separator is used to lower the cell short risk.

4. Conclusion

The intricate interplay between SEI layers and Li growth critically affect the cycling stability and safety of Li metal anode. Two different cell failure mechanisms, i.e., cell impedance buildup and dendrite-caused cell short are decoupled simply by using highly porous glass fiber as the separator. Conflicting requirements on SEI properties are identified to improve reversible Li cycling and stop dangerous Li dendrite growth. A quantification method based on EIS has been developed to quickly evaluate the SEI properties derived from various electrolytes, providing an effective protocol for electrolyte comparison and selection. A widely applicable Li growth mechanism in different electrolytes has been proposed which explains well the observed Li morphology evolution reported in literature. New insights have been provided to address the challenges in enabling safe and reversible Li metal anode for high energy battery technologies.

Acknowledgements

The authors acknowledge support from the National Science Foundation (NSF) under Grant No. CBET-1748279. T.T. was supported by Summer Internship at University of Arkansas through NSF-sponsored EEC-1359086. The authors also thank Zhangjiagang Guotai Huarong New Chemical Materials Co., Ltd. in China for providing electrolytes used in this work.

Appendix A. Supplementary material

Supplementary data associated with this article can be found in the online version at http://dx.doi.org/10.1016/j.nanoen.2017.08.005.

References

[1] D. Lin, Y. Liu, Y. Cui, Nat. Nanotechnol. 12 (2017) 194–206.
[2] A. Varzi, R. Raccichini, S. Passerini, B. Scrosati, J. Mater. Chem. A 4 (2016) 17251–17259.
[3] J.B. Goodenough, ACS Catal. 7 (2017) 1132–1135.
[4] X.-B. Cheng, R. Zhang, C.-Z. Zhao, F. Wei, J.-G. Zhang, Q. Zhang, Adv. Sci. 3 (2016) (1500213-n/a).
[5] M.S. Whittingham, Proc. IEEE 100 (2012) 1518–1534.
[6] D. Aurbach, E. Zinigrad, Y. Cohen, H. Teller, Solid State Ion. 148 (2002) 405–416.
[7] D. Lv, J. Zheng, Q. Li, X. Xie, S. Ferrara, Z. Nie, L.B. Mehdi, N.D. Browning, J.-G. Zhang, G.L. Graff, J. Liu, J. Xiao, Adv. Energy Mater. 5 (2015) 1402290.
[8] X.-B. Cheng, C. Yan, J.-Q. Huang, P. Li, L. Zhu, L. Zhao, Y. Zhang, W. Zhu, S.-T. Yang, Q. Zhang, Energy Storage Mater. 6 (2017) 18–25.
[9] C.-P. Yang, Y.-X. Yin, S.-F. Zhang, N.-W. Li, Y.-G. Guo, Nat. Commun. 6 (2015) 8058.
[10] K.N. Wood, E. Kazyak, A.F. Chadwick, K.-H. Chen, J.-G. Zhang, K. Thornton, N.P. Dasgupta, ACS Cent. Sci. 2 (2016) 790–801.
[11] R. Chianelli, J. Cryst. Growth 34 (1976) 239–244.
[12] D. Aurbach, J. Power Sources 89 (2000) 206–218.
[13] M. Wu, J. Jin, Z. Wen, RSC Adv. 6 (2016) 40270–40276.
[14] J. Qian, W.A. Henderson, W. Xu, P. Bhattacharya, M. Engelhard, O. Borodin, J.-G. Zhang, Nat. Commun. 6 (2015) 6362.
[15] K.J. Harry, D.T. Hallinan, D.Y. Parkinson, A.A. MacDowell, N.P. Balsara, Nat. Mater. 13 (2014) 69–73.
[16] H. Wu, D. Zhuo, D. Kong, Y. Cui, Nat. Commun. 5 (2014) 5193.
[17] G. Zheng, S.W. Lee, Z. Liang, H.-W. Lee, K. Yan, H. Yao, H. Wang, W. Li, S. Chu, Y. Cui, Nat. Nanotechnol. 9 (2014) 618–623.
[18] F. Ding, W. Xu, G.L. Graff, J. Zhang, M.L. Sushko, X. Chen, Y. Shao, M.H. Engelhard,

Z. Nie, J. Xiao, X. Liu, P.V. Sushko, J. Liu, J.-G. Zhang, J. Am. Chem. Soc. 135 (2013) 4450–4456.
[19] Celgard LLC, Battery Separator Products, 2017 ⟨https://www.celgard.com/literature⟩, (Accessed 20 March 2017).
[20] F. Sun, R. Moroni, K. Dong, H. Markötter, D. Zhou, A. Hilger, L. Zielke, R. Zengerle, S. Thiele, J. Banhart, I. Manke, ACS Energy Lett. 2 (2017) 94–104.
[21] R. Guo, L. Lu, M. Ouyang, X. Feng, Sci. Rep. 6 (2016) 30248.
[22] Q. Wang, J. Zheng, E. Walter, H. Pan, D. Lv, P. Zuo, H. Chen, Z.D. Deng, B.Y. Liaw, X. Yu, J. Electrochem. Soc. 162 (2015) A474–A478.
[23] K.H. Wujcik, T.A. Pascal, C. Pemmaraju, D. Devaux, W.C. Stolte, N.P. Balsara, D. Prendergast, Adv. Energy Mater. 5 (2015) 1500285.
[24] Y. Yamada, K. Furukawa, K. Sodeyama, K. Kikuchi, M. Yaegashi, Y. Tateyama, A. Yamada, J. Am. Chem. Soc. 136 (2014) 5039–5046.
[25] D. Lu, J. Tao, P. Yan, W.A. Henderson, Q. Li, Y. Shao, M.L. Helm, O. Borodin, G.L. Graff, B. Polzin, C.-M. Wang, M. Engelhard, J.-G. Zhang, J.J. De Yoreo, J. Liu, J. Xiao, Nano Lett. 17 (2017) 1602–1609.
[26] G. Bieker, M. Winter, P. Bieker, Phys. Chem. Chem. Phys. 17 (2015) 8670–8679.
[27] P. Arora, Z. Zhang, Chem. Rev. 104 (2004) 4419–4462.
[28] Celgard LLC, Battery Inovation, 2017 ⟨https://www.celgard.com/battery-innovation/⟩, (Accessed 20 March 2017).
[29] F. Orsini, A. Du Pasquier, B. Beaudoin, J.M. Tarascon, M. Trentin, N. Langenhuizen, E. De Beer, P. Notten, J. Power Sources 76 (1998) 19–29.
[30] S.-i. Tobishima, K. Takei, Y. Sakurai, J.-i. Yamaki, J. Power Sources 90 (2000) 188–195.
[31] K. Xu, Chem. Rev. 104 (2004) 4303–4418.
[32] M. Nie, D.P. Abraham, D.M. Seo, Y. Chen, A. Bose, B.L. Lucht, J. Phys. Chem. C 117 (2013) 25381–25389.
[33] L. Suo, O. Borodin, T. Gao, M. Olguin, J. Ho, X. Fan, C. Luo, C. Wang, K. Xu, Science 350 (2015) 938–943.
[34] J. Zheng, J. Lochala, A. Kwok, Z.Z. Deng, J. Xiao, Adv. Sci. 1700032 (2017).
[35] Q. Ma, Z. Fang, P. Liu, J. Ma, X. Qi, W. Feng, J. Nie, Y.-S. Hu, H. Li, X. Huang, L. Chen, Z. Zhou, ChemElectroChem 3 (2016) 531–536.
[36] Y.S. Cohen, Y. Cohen, D. Aurbach, J. Phys. Chem. B 104 (2000) 12282–12291.
[37] M.D. Tikekar, S. Choudhury, Z. Tu, L.A. Archer, Nat. Energy 1 (2016) 16114.